POLITECNICO DI TORINO
Repository ISTITUZIONALE

Thermal design and analysis of a nanosatellite in low earth orbit

(Article begins on next page)

04 August 2020

Author's Accepted Manuscript

Thermal design and analysis of a nanosatellite in low earth orbit

S. Corpino, M. Caldera, M. Masoero, F. Nichele, N. Viola
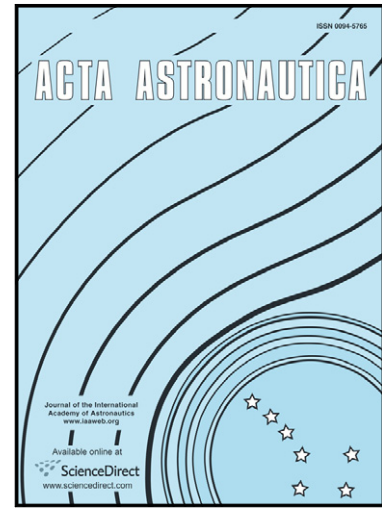
Cite this article as: S. Corpino, M. Caldera, M. Masoero, F. Nichele, N. Viola, Thermal design and analysis of a nanosatellite in low earth orbit, *Acta Astronautica,* http://dx.doi.org/10.1016/j.actaastro.2015.05.012

Thermal design and analysis of a nanosatellite in low Earth orbit

S. Corpino[*1a]

sabrina.corpino@polito.it

Contact Person. Mobile: 0039 3358383181. Tel: 0039 0110906867

M. Caldera[2b]

matteo.caldera@enea.it

M. Masoero[3c]

marco.masoero@polito.it

F. Nichele[1d]

fabio.nichele@polito.it

N. Viola[1a]

nicole.viola@polito.it

[1] Department of Mechanical and Aerospace Engineering, Politecnico di Torino, Torino, Italy

[2] Agenzia nazionale per le nuove tecnologie, l'energia e lo sviluppo economico sostenibile (ENEA), Italy

[3] Department of Energy, Politecnico di Torino, Torino, Italy

[*a] Assistant professor, Corresponding author

[a] Assistant professor

[b] Research associate

[c] Full professor

[d] PhD candidate

Abstract

In this paper, we present the process and the results of the thermal analysis applied to a nanosatellite developed at Politecnico di Torino. First, main mission parameters and the spacecraft design are presented, in order to fix the boundary conditions and the thermal environment used for the analysis. Then, the thermal model built to solve the thermal balance problem is described into details, and the numerical simulation code is presented. Finally, results are given and discussed in depth. The tool developed provides excellent modelling capabilities and temperature distributions have been validated through commercial software.

The analysis has been used to refine the spacecraft configuration and to set the requirements applicable to the thermal control system of the satellite. The results showed that a basically passive control is sufficient to maintain most spacecraft's components within their temperature range when appropriate thermal coatings and/or tapes are provided. However, heaters to warm up batteries are recommended to survive coldest conditions.

1. **Introduction**

In the last few years, small satellites have changed the landscape of space missions. The small satellites category includes space platforms that weigh less than 1000 kg, and within this category further subdivisions do exist, as reported in [1]. In the present paper we refer specifically to nanosatellites, i.e. satellites whose mass does not exceed ten kg. These space platforms have two main inherent advantages: 1) the cost, which is low if compared to that of traditional satellites; 2) the time for development, which is generally one order of magnitude lower than that of bigger systems and more complex missions. However, these space platforms do also have criticalities mainly related to their performance and reliability [2]. To accomplish ambitious mission goals, a set of technological challenges need to be addressed. Design processes, and verification and operation activities will also require specific advancement.

In the framework of small satellites, nanosatellites developed in universities for educational, scientific and technological purposes are worth mentioning [3]. Main aims of these initiatives are:

- to engage students in a challenging team work, which is aimed at the design, development and manufacturing of a complex product, thus training the students' capability of solving real problems
- to test in orbit components and materials designed for terrestrial use, in order to pursue cost reduction of future space missions
- to demonstrate the feasibility of innovative missions and systems concepts

The process of development of University satellites follows that of traditional space products but it applies alternative methods and resources, in order to keep costs and development times down and to make the process suitable to personnel with developing skills, i.e. students. To this purpose, the CubeSat standard was created in 1999 at California Polytechnic State University and Stanford University [4]. The basic CubeSat unit (1U) is a 10cm-side cube-shaped platform whose mass is less than 1.33 kg, complying with the CubeSat Design Specification [5]. One of the most crucial issues for nanosatellite missions is the effect of the thermal environment on the satellite. University satellites, because of their own nature (costs, size, developers), have generally a full (or almost full) passive Thermal Control System (TCS). Moreover, taking into account the limited budget, simple technical solutions and Commercial-Off-The-Shelf (COTS) components, i.e. components available on the market, are usually adopted in design and manufacturing. Without vehicles dedicated to launching CubeSats as primary payloads, launch opportunities only exist in the form of secondary payload missions. This implies that the orbit is not chosen by the CubeSat developer and that the mission's starting date is not known well in advance. Eventually, as far as thermal issues are concerned, there is always the need to optimize the costly test campaign, in order to reduce its impact on the development time and costs of the satellite. The capability of performing effective and reliable thermal analyses represents therefore a fundamental role in the design of the TCS and of the whole satellite.

The paper describes the results of a theoretical and numerical study, aimed at assessing the thermal conditions and the range of operative temperatures encountered by a nanosatellite in orbit.

Thermal analyses are usually conducted by means of commercial energy-balance software, e.g. multi-physics tools that couple computational fluid dynamics (CFD) and finite elements method (FEM) analyses. Even though a powerful set of referenced tools available on the market provide detailed results and a variety of post-processing options, the creation and implementation of in-house software has the advantage to give the analyst the ability to tailor and optimise the model to the actual case study. CFD models are limited for space application since the atmosphere is rarefied and the heat transfer phenomena are regulated mainly by thermal conduction and radiation. Furthermore, the available FEM tools usually are not easily adaptable to the nanosatellite scale, and the license fee of commercial software is generally expensive. For these reasons, the development of an in-house numerical code has been preferred for the purpose of this study.

The simulation code has been developed in MATLAB® environment, and it solves the thermal energy balance of a nanosatellite in LEO through the finite difference numerical approach. The model is three-dimensional and time dependent. Both external radiation, i.e. direct solar radiation, albedo, Earth Infra-Red (IR) radiation, and internal heat generation, due to the on-board electronics, are modelled.

The goal of the implemented numerical model is to calculate the temperature profile of the satellite under dynamic conditions and especially to evaluate the compliance with the operative limits of the

most critical electronic equipment in the design orbits, i.e. the reference warm and cold orbits. The same reference scenarios were analysed for comparison of results obtained via thermal software ESATAN-TMS®.

The analysis has been applied to the PiCPoT project [6] described into some detail in Section 2. The statement of the thermal problem is given in Section 3, where requirements and constraints, the environment and the boundary conditions are given. The methodology and the implemented algorithms are tailored on a mesh specific to the nanosatellite, as described in Section 4. The model is versatile and many parameters and input data can be varied from the user interface. The results are displayed in graphical form and collected in output files that can be imported in spread-sheet software for further analysis. Moreover a video is created in .avi format to show the time evolution of the temperature profile of the nanosatellite. The video automatically updates during the numerical simulation and can be read by any media player. The results are shown and discussed in Section 5, where the validation of the code through a commercial software is also summarised. Eventually, some conclusions and suggestions for future works are drawn in Section 6.

2. The reference mission and satellite

PiCPoT nanosatellite has been developed in the framework of a university program and pursues mainly educational but also scientific and technological purposes, in line with this kind of initiatives. In the following paragraphs main mission features and satellite configuration are described into some detail to better understand the assumptions taken in the thermal analysis.

2.1. Mission objectives

Primary objective of the PiCPoT mission is to educate undergraduate and graduate students on space missions design and development. The goal is pursued by setting up a permanent hands-on education program based on satellites projects and laboratory activities.

The main technical objective of the PiCPoT mission is taking pictures of the Earth and transmitting them to ground . Additional goals are in-orbit demonstration of materials and COTS equipment (e.g. cameras), originally developed for terrestrial use, and in-orbit verification of the operation of a brushless DC motor, used as reaction wheel.

2.2. Orbit

The initial values of orbital parameters, necessary to predict PiCPoT orbit, are affected by a certain degree of uncertainty. However it is known that PiCPoT will travel along a circular sun-synchronous orbit with an altitude of 600 km and an inclination equal to 98 deg ($\pm$ 0.04 deg) [7]. In case the RAAN and the date of release in orbit are unknown, the β angle (i.e. the angle between the orbital plane and the Sun-Earth line) shall be assumed to be variable in the range $0 \div 90$ deg.

2.3. Attitude

Taking into account the mission objectives and the related requirements, the orbit imposed by the launch vehicle and the constraints due to the development of a low cost satellite, permanent magnets and hysteresis devices have been selected as passive attitude control means.. The choice was also driven by the geometry of the satellite, the limitations in mass and volume and considering the favourable orientation of the Earth magnetic field in the geographical area of interest . In particular, permanent magnets are useful to generate control torques to orient the body axis of the satellite along which permanent magnets are located along the Earth magnetic field lines. Hysteresis bars are useful to damp oscillations that the satellite experiences immediately after being released from the launcher, all over the orbit and particularly twice per orbit when it flies over the Earth poles. In order to take pictures of the Earth northern hemisphere and to meet the pointing requirement, PiCPoT cameras have therefore to be aligned along the same body axis of the permanent magnets. Thus, the surface of the cube where the cameras' lenses are located, faces the Earth when the satellite flies over the Earth's northern hemisphere. The passive magnetic attitude control system guarantees only two-axis stabilization of the satellite, which can rotate freely around the -x body axis. The two-axis control allows matching the objective of the PiCPoT mission. However, one reaction wheel is placed along the x-body axis to control the third degree of freedom.

2.4. Satellite's configuration

PiCPoT nanosatellite is characterised by a simple mechanical architecture. It is a cube with a side of 130 mm and a mass of 2.5 kg and consists of rods and panels, which are screwed together to form the external structure of the satellite, as shown in Figure 1 and Figure 2. The faces of the satellite are named upon their orientation with respect to the body reference frame (Figure 2), as summed up in Table 1.

Perpendicular axis and direction	Name
+x	F0
-x	F5
+y	F1
-y	F3
+z	F2
-z	F4

Table 1: faces nomenclature

All structural elements are manufactured in Aluminium alloy with an alodine surface treatment.

Five out of six external faces of PiCPoT are covered with Gallium Arsenide Triple Junction solar cells. The bottom panel and the launcher interface plate are screwed together. Two antennas, both for uplink and downlink communications, are attached to the latter plate: one low frequency double helical antenna (435 MHz) and one s-band patch antenna (2.4 GHz). There are also three camera lenses and two

deployment switches (Figure 2) to guarantee the satellite is switched off during launch and ascent to orbit. The launcher interface plate has a square shape with two machined tips, which are used to fix the satellite to the launcher adapter. PiCPoT internal support structure is constituted by four C-section plates. The top, the bottom and the four C-sections panels are all screwed together. The internal structure is the framework for battery packages and electronic boards, as shown in Figure 3. PiCPoT has two different types of batteries, Nickel-Cadmium (NiCd) and Lithium-Polymer (LiPo), for a total of six battery packages. The well known NiCd demonstrated to operate properly in space, and are sufficient to supply the on-board systems in the nominal operative mode. The LiPo packs are part of the technological experiment, as they have not yet been thoroughly tested on a large scale in orbit.
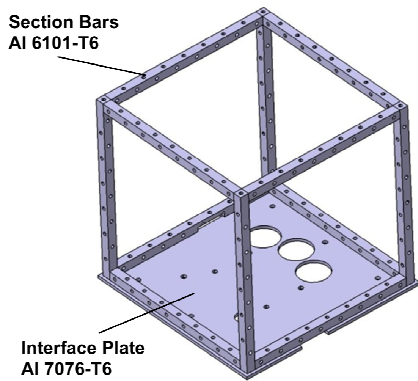
Figure 1: main structure
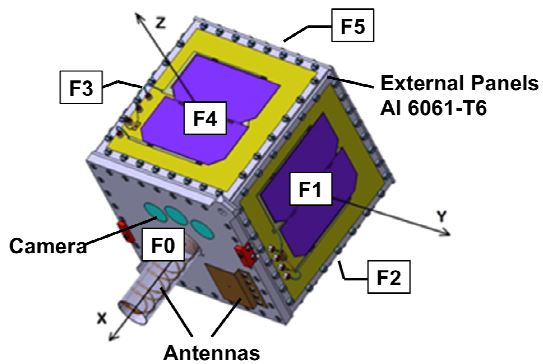
Figure 2: interface plate with antennas, cameras' lenses and kill switches. Body reference frame is shown

Figure 3: internal structure, batteries, and harness

Figure 4: internal structure and avionics layout

As far as on-board systems are concerned, they encompasses six interconnected electronic boards that perform the following functions:

- electrical power management (Power Supply and Power Switch)
- command and data handling (Processor A and Processor B)

- communications (RxTx)
- payload management (Payload)

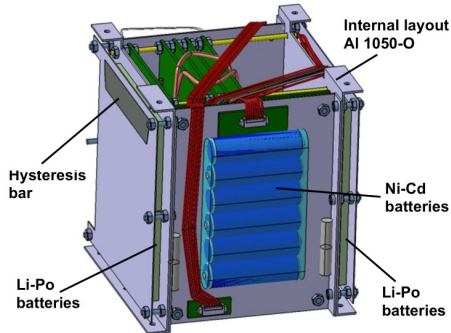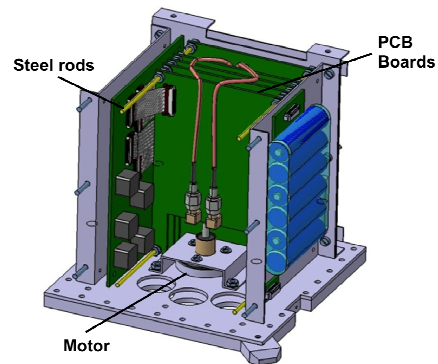The brushless DC motor (Figure 4), working as reaction wheel, is located on the bottom panel of the satellite. Four permanent magnets are placed on the C-section panels near the NiCd batteries (Figure 3), whereas two hysteresis plates are glued on the two opposite panels, which enclose the LiPo batteries. The three cameras are screwed to the bottom panel in correspondence to the holes depicted in Figure 4.

3. Thermal analysis: objectives and problem definition

The thermal analysis identifies the external and internal heat sources of the satellite and predicts the temperature ranges of structures, solar panels, electronic boards and equipment, in order to evaluate whether or not they remain within the operational and survival limits throughout the mission in all operative modes. In case the temperature requirements are not met, different equipment and components may be selected or design changes may be considered to guarantee the correct operation of the satellite. Guidelines and methods for satellites' thermal analysis and TCS design are extensively discussed in [8] and [9].

3.1. Thermal management solutions

The main function of thermal control is to maintain satellite equipment within the required temperature limits, through the identification of appropriate thermal control techniques and hardware, according to the complexity and the category of the satellite. Thermal control techniques may be either passive or active but the former is the most widespread option for small university satellites. References [10]-[16] show interesting examples of thermal control systems adopted on-board small platforms.

Passive thermal control relies mainly on the definition of the architecture and layout of the satellite, and makes use of materials, coatings or surface finishes, thermal insulation and heat sinks with adequate thermo-optical properties. Surface finishes may be used both on the interior and on the external surfaces of the nanosatellite, for the purpose of enhancing thermal radiative exchange. In particular external surfaces shall be able to achieve the energy balance at the desired temperatures between spacecraft internal dissipation, external heat sources, and re-radiation to space. The external radiative exchange depends on. solar absorptivity and infrared emissivity of the surfaces. Two or more coatings may be combined to obtain the desired values of absorptivity and emissivity, taking into account the compatibility between coating and substrate, their resistance to contamination and in-space degradation (for a detailed discussion on thermal control coatings, reference to [17] [18]).

Thermal insulation aims at reducing thermal exchange between two adjacent surfaces at different temperatures. Thermal insulation can be achieved either with homogeneous materials (for instance foam with low thermal conductivity) or with multilayer insulation systems (layered blanket), constituted by multiple layers of low-emittance films, metallized on both surfaces with aluminium or gold [19]. Multilayer insulation are widely used for satellite's thermal control with the following purposes:

- to prevent excessive thermal flux from/to components
- to reduce temperatures variation due to environmental radiative fluxes that vary considerably with time
- to minimize temperature gradients

Heat sinks are high thermal capacitance materials that minimize temperature gradients of adjacent components, and are widely used for electronic devices with cycling operation.

As far as the active thermal control is concerned, one of the main techniques used on board nanosatellites consists in the use of heaters. Heaters are basically resistors that protect components from cold-case conditions, for instance keeping batteries temperature over the minimum operating limit. Heaters are usually part of a closed-loop system that includes sensors and controller, and they operate according to the desired logic.

Simplicity and flexibility are the key drivers for the choice of the most appropriate thermal control techniques. In the present case, we first assumed a purely passive thermal control system. Objectives of the thermal analysis, presented in Section 5, are the definition and the verification of the designed thermal control system to ensure that the thermal requirements of all components are met. In case thermal requirements are not fully met and problems arise at system level, the following actions may be implemented:

- variation of satellite's internal layout. This solution depends however on the phase of the satellite's life-cycle and on the constraints imposed by satellite's geometry and masses distribution
- variation of surface finishes. This solution depends on the thermo-optic properties of materials available on the market
- change of materials. This solution depends on the phase of the satellite's life-cycle. Moreover, it is also limited by the availability of materials that may be either already in house or anyway easily accessible on the market

In case problems arise at subsystem or component level, the following actions may be implemented:
- installation of heaters on components that need to be warmed up
- installation of heat sinks for components that need to be cooled down
- selection of components with the appropriate temperature range.

3.2. Thermal environment definition

The external boundary conditions are mainly characterised by the orbital parameters, by the position of the Earth on the ecliptic (epoch) and by the external radiation sources, i.e. the direct solar radiation, the albedo and the Earth Infra Red (IR) radiation.

The direct solar radiation depends on the solar constant S_0 = 1367 W/m^2, defined as the intensity of sunlight radiation perpendicular to a surface at the Earth's mean distance from the Sun (1 AU). However, because of the Earth orbit eccentricity (e), the solar radiation is inversely proportional to the Earth's distance from the Sun and, specifically, it ranges from a minimum value of $S_0/(1+e)^2$ = 1322 W/m^2 at aphelion to a maximum value of $S_0/(1-e)^2$ = 1414 W/m^2 at perihelion, with a percentage variation of ±3.4% [20]. Guidelines for the selection of parameters useful to schematically represent external heat sources are provided in [21] [22].

Nanosatellite's internal heat sources are represented by the on board electronics: electronic boards, batteries, cameras and the reaction wheel (i.e. the brushless DC motor). Depending on the operative modes, the internal heat dissipation varies according to the duty cycle of the electronics. Values of

power dissipation have been estimated for the electronic boards, and their duty cycle along the orbit has been considered.

The six battery packages are never operating simultaneously, but are sequenced such that in turn one is charging, two are discharging and the remaining three battery packages are switched off. Battery packages are divided into two groups; in particular the two battery packages that are discharging belong to two different chains, in order to guarantee functional redundancy. As far as the temperature operational limits are concerned, batteries are the most critical components, as reported in Table 2.

Name	Function	Component	Power [W]	Operating time/orbit	Temperature [°C]	
					min	max
S0	EPS	Power Supply	30% solar panels power	full time	-20	+85
S1	RxTx	Amplifier 1	4.00	10 minutes	-30	+100
		Amplifier 2	1.35	10 minutes	-30	+100
S2	EPS	Power Switch	2.40	10 minutes	-20	+85
S3	OBC	Proc. A	0.03	full time	-40	+85
S4	Payload	Board	1.00	10 seconds	-40	+85
		Camera	0.50	5 seconds	-20	+80
S5	OBC	Proc. B	0.03	full time	-40	+125
M	Payload	Motor	3.00	10 minutes		
B1/B3	EPS	Battery (NiCd)	1.00	Charge (Ref. Fig. 5b)	0	+70
			0.50	Discharge (Ref. Fig. 5b)	-20	+70
			0.00	Storage	-30	+70
B2/B4	EPS	Battery (LiPo)	1.50	Charge (Ref. Fig. 5b)	0	+45
			1.10	Discharge (Ref. Fig. 5b)	-20	+60
			0.00	Storage	-20	+60

Table 2: on-board electronic equipment dissipation and temperature range

The brushless DC motor dissipates heat only when it is switched on a few times during the mission, as it is a secondary payload activated upon command from ground. Taking into account the low power dissipation of cameras and of their duty cycle, they have been neglected as internal heat sources.

Table 2 shows the temperature ranges of the on-board electronic equipment and gives an indication of the maximum heat dissipation for each component. Figure 5 illustrates the variation of internal power dissipation along two orbits. In particular, it represents the power dissipated by the electronic boards and the motor (left-hand chart) and the batteries (right-hand chart), as a function of time in the worst cold case. The most important contributions in terms of heat generated are caused by S0, S1 and S2.
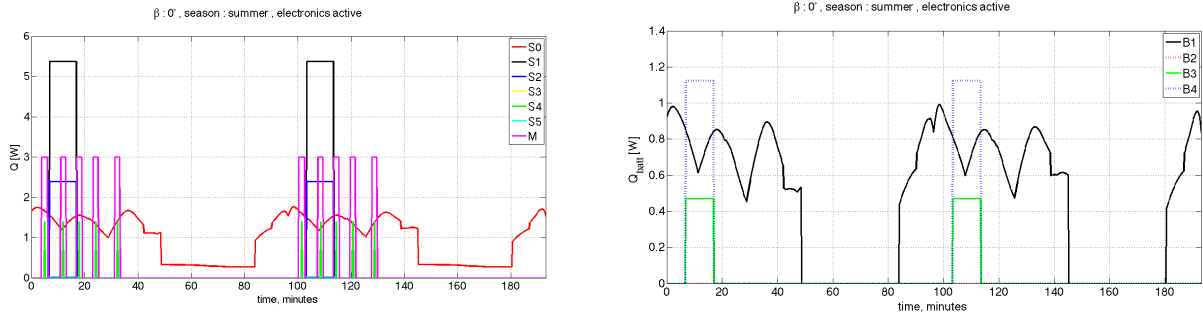
Figure 5: heat loss from the electronics and the brushless motor (left) and batteries (right). (2 orbits, height 600 km, i = 98 deg, β = 0 deg, Earth @aphelion)

4. **Thermal analysis: methodology**

In this section the numerical code developed to carry out the thermal analysis is described into detail, after presenting and discussing the assumptions, and introducing the numerical methods. Symbols used in the following paragraphs are listed in Appendix A at the end of paper.

4.1. Models of orbit and heat loads

Albedo and Earth IR radiation vary with position in space and time and depend on radiation wavelength and other uncertain factors (e.g. weather conditions) [23]. The following simplifying hypotheses have been assumed in the present thermal analysis. In particular Earth's reflectivity and emissivity have been considered:

- isotropic and diffuse (Lambertian reflector and emitter)
- independent of wavelength
- constant throughout the mission

Suitable average design values of albedo and Earth IR radiation are obtained from the 1st Law of Thermodynamics applied to the Earth throughout one year:

- $\alpha = 0.29$
- $IR = 239 \ W/m^2$

The heat flux on the satellite's external surfaces depends on geometrical factors and on the orientation of the satellite relative to the heat sources (Earth and Sun).

The albedo heat flux is given by the following formulas:

$$\dot{q}_{\alpha,j} = S \cdot f(\theta,\iota) \cdot \cos\left(\frac{\pi}{2\gamma_{\lim}}\gamma_j\right) \qquad \text{if} \ \ |\gamma_j| < \gamma_{\lim} \tag{1}$$

$$\dot{q}_{\alpha,j} = 0 \qquad \text{if} \ \ |\gamma_j| \geq \gamma_{\lim} \text{ or } \theta > \pi/2 \tag{2}$$

where the intensity of albedo $S \cdot f(\theta, \iota)$ is a function f of the orbital angles θ and ι and:

- γ_j is the angle between the Earth-satellite vector and the perpendicular to the j-th external face of the satellite
- γ_{lim} is the angle between the Earth-satellite vector and the direction beyond which the satellite's faces are not anymore in view of the Earth
- θ is the solar zenith angle, which is the angle between the Earth-satellite and the Earth-Sun directions and can vary between 0 deg and 180 deg
- ι is the angle between the Earth-satellite vector and the tangent to the Earth viewed from the satellite; it is a constant value for circular orbits, once the orbit's altitude has been fixed

Similarly the IR heat flux can be calculated with the following formulas:

$$\dot{q}_{IR,j} = IR \cdot \cos\left(\frac{\pi}{2(\pi/2+\iota)} \gamma_j \right) \qquad \text{if } |\gamma_j| < (\pi/2 + \iota) \tag{3}$$

$$\dot{q}_{IR,j} = 0 \qquad \text{if } |\gamma_j| \ge (\pi/2 + \iota) \tag{4}$$

The solar flux incident on the j-th face is zero if the face is opposite to the Sun or if it is eclipsed by the Earth. For a satellite on a circular orbit the latter case occurs when two conditions apply simultaneously: $\theta > 90$ deg and $R \sin(\theta) < R_E$ (R is the distance between the satellite and the Earth's centre, whose radius is R_E). In all other cases the solar flux incident on the j-th face is given by:

$$\dot{q}_{sun,j} = S \cdot \cos \varsigma_j , \text{ with } \cos\varsigma_j > 0 \tag{5}$$

$$\dot{q}_{sun,j} = 0 , \text{ with } \cos\varsigma_j \le 0 \tag{6}$$

where ς_j is the angle between the perpendicular to the j-th face and the vector opposite to Sun rays.
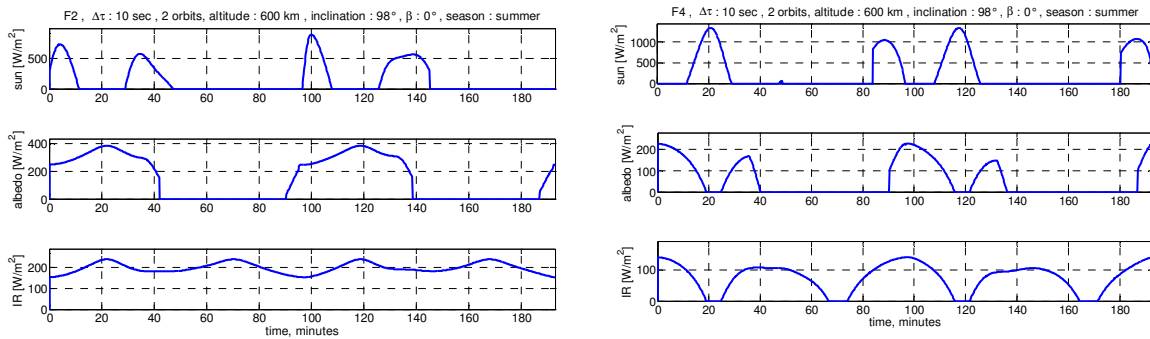

Figure 6: incident external radiation on F2 and F4: solar radiation, albedo and Earth IR radiation (2 orbits, height 600 km, i = 98 deg, worst cold orbit)
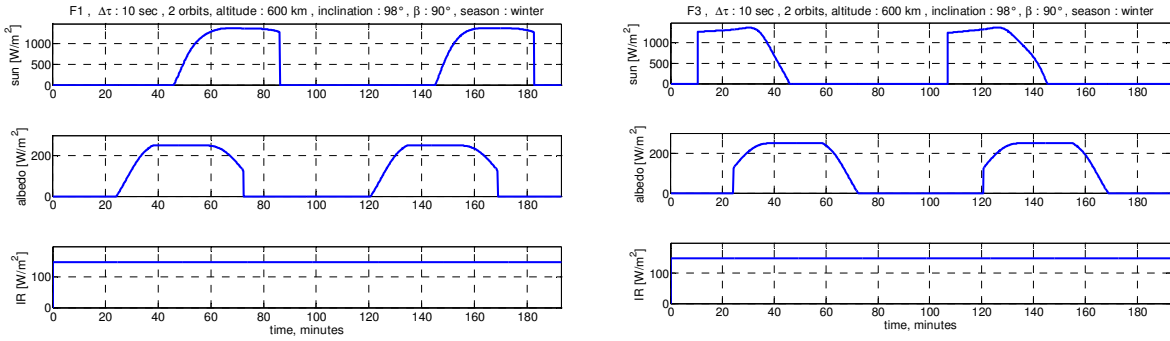
Figure 7: incident external radiation on F1 and F3: solar radiation, albedo and Earth infrared radiation (2 orbits, height 600 km, i = 98 deg, worst hot orbit)

Once the orbital elements are established and heat fluxes are estimated, a set of orbits can be considered for the analysis. The approach requires to consider first the condition of maximum and minimum external heat fluxes for the design orbits (*worst hot* and *cold orbit*), then the internal heat rate is accounted to determine the ultimate design cases: *worst hot case* and *worst cold case.* The cold orbit occurs when the satellite is for the longest time shadowed by the Earth (eclipses), hence is cooled down most (orbit type Noon-Midnight), while the hot orbit occurs when the duration of the eclipse is minimal (orbit type Dawn-to-Dusk).

One of the characteristic parameters of the design orbits is the β-angle, which is the angle between the orbit plane and the Sun-Earth vector direction. A Noon-Midnight orbit type is featured by β = 0 deg, while β = 90 deg denotes a Dawn-to-Dusk orbit type. The second parameter affecting the design orbits is the position of the Earth on the ecliptic, defining the distance of the Earth from the Sun.

Eventually, taking into account also the internal heat generation, we may say that the worst cold and hot design cases are:

a. *Worst cold case*: β = 0 deg, Earth located at aphelion, on-board electronics turned off
b. *Worst hot case*: β = 90 deg, Earth located at perihelion, on-board electronics turned on

Figure 6 and Figure 7 derive from running the numerical simulation code and illustrate the time evolution of the heat flux impinging the external faces of the nanosatellite along two orbits, for the two cases cited above. The behaviour of the heat fluxes on the satellite is strongly influenced by the attitude dynamics along the orbit. Regarding the direct solar radiation, if a face points towards the Sun, the opposite face is "in eclipse". For the albedo and the IR the behaviour is less intuitive. For example, with reference to Figure 6, when F4 is facing the Sun (solar flux is maximum), F2 is pointing the nadir (albedo and IR fluxes reach the maximum on F2 while they tend to zero for F4). The plots in Figure 7 are quite different from those depicted in Figure 6 due to the different orbit assumed for the worst hot case. It can be noticed that the IR contribution is almost constant along the orbit due the specific geometry of a dawn to dusk orbit.

The heat rate absorbed by the solar cells is represented in Figure 8 as a function of time for the design orbits, considering all three types of radiation and only the solar contribution (direct and albedo). It can also be noticed from these graphs that the eclipse duration decreases as the β angle increases.

The MATLAB® functions created are flexible and allow to modify many parameters for each electronic component, e.g. the heat dissipated, and the duty cycle. The details are described in Section 4.3.
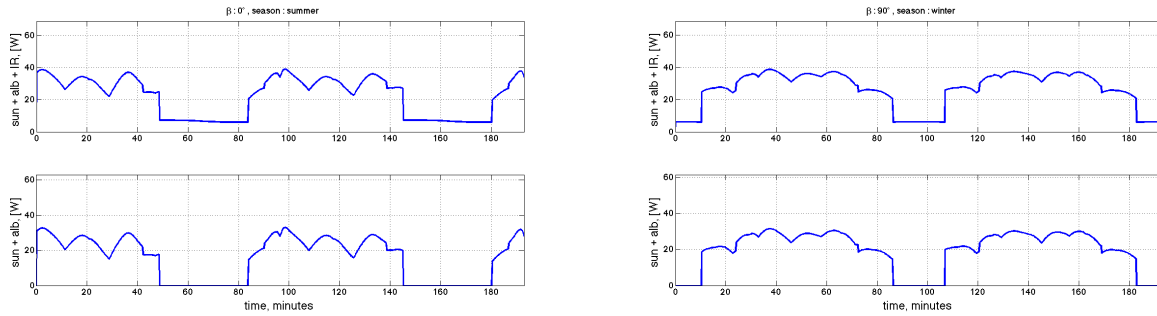

Figure 8: incident radiation on solar cells for the worst cold orbit (on the left) and worst hot orbit (on the right): incident radiation from all sources (upper graphs) and from Sun (direct+albedo) (lower graphs) (2 orbits, height 600 km, i = 98 deg)

4.2. The heat transfer model

Heat transfer in the satellite is basically the result of conjugate thermal conduction and radiation. Temperatures vary along the three dimensions and are time-dependent.

Thermal conduction is evaluated with the assumptions that materials are homogenous with constant thermal conductivity, with the only exception of the Kapton® multilayer insulation. These assumptions are acceptable due to the temperature range experienced by the satellite in orbit. Heat conduction is modelled by the Fourier's equation:

$$a\nabla^2 T + \frac{\dot{q}_v}{\rho \cdot c} = \frac{\partial T}{\partial \tau} \tag{7}$$

Thermal radiation among the cavities into which the internal volume of the satellite is divided, is modelled with the Absorption Factors Method, which can be easily implemented in a numerical code [24] [25] [26]. The absorption factor $B_{i,j}$ represents the fraction of energy emitted by surface i that is absorbed by surface j. Surfaces are assumed opaque and grey. In a cavity delimited by n grey, opaque and diffuse surfaces filled with non-participating media, the algebraic equations that link $B_{i,j}$ and Q_i are:

$$\sum_{i=1}^{n} \left(F_{pi} r_i - \delta_{pi} \right) B_{ij} + F_{pj} \varepsilon_j = 0 \tag{8}$$

$$\dot{Q}_i = \dot{q}_{\varepsilon,i} A_i - \sum_{j=1}^{n} B_{ji} \dot{q}_{\varepsilon,j} A_j \tag{9}$$

Subscript p varies from 1 to n for a given j, and then j varies from 1 to n, giving rise to n^2 equations. The reflectivity is the complement to 1 of the emissivity, $\rho = 1 - \varepsilon$. Equation (8) is written for each p-th surface, and letting j take on all values from 1 to n, a set of linear equations in the unknown quantity B_{ij} is obtained and solved simultaneously.

Once absorption factors are known, equation (9) allows to calculate temperatures of the surfaces, as explained in Section 4.3. $\dot{Q}_i$ is the net radiative heat rate of i-th surface A_i, while $\dot{q}_{\varepsilon,i}$ is the heat flux emitted by the same surface.

4.3. The numerical algorithm

The thermal analysis of the nanosatellite is accomplished through a numerical code that has been implemented in MATLAB® environment. Analytical equations are discretised by the finite difference approach and a fully implicit iterative scheme (Laasonen method). A detailed description of the numerical models can be found in [27] [28].

The fully implicit scheme is not affected by instability issues related to limitations of the time step. Therefore, the time step of 10 s has been selected in order to guarantee adequate results with limited computation time and hardware requirements.

The external surfaces of the satellite are modelled with an uniform hexa grid, while each component of the electronic equipment is modelled as a lumped node, and the mounting bars are modelled as 1D elements.

The initial temperature is set to 273.15 K for all nodes. This assumption influences mainly the first orbit, while it has a negligible influence on the next orbits.

The temperature of node (i, j, k) placed on the external structure of the satellite evaluated at future time l+1 is:

$$T_{i,j,k}^{(l+1)} = C_f \cdot \begin{pmatrix} T_{i,j,k}^{(l)} + Fo\left(T_{i+1,j,k}^{(l+1)} + T_{i-1,j,k}^{(l+1)} + T_{i,j+1,k}^{(l+1)} + T_{i,j-1,k}^{(l+1)}\right) + \\ + h_g \cdot C_t \cdot T_{int}^{(l+1)} + \left(\dot{q}_s - \varepsilon \cdot \sigma \cdot (T_{i,j,k}^{(l)})^4\right) \cdot C_t \end{pmatrix} \tag{10}$$

The equation is slightly different for nodes placed on the border and vertex of the structure, in order to account for the interaction of the neighbouring faces.

In equation (10) T_{int} is the temperature of the corresponding internal node, $\dot{q}_s$ is the external heat flux absorbed by the node, and h_g is the thermal conductance of Kapton® multilayer insulation placed between the external and internal structure. The following coefficients highlight specific contributions to the energy balance:

$$Fo = a \cdot \frac{\Delta\tau}{d^2} \tag{11}$$

$$C_t = \frac{\Delta\tau}{\rho \cdot c \cdot s} \tag{12}$$

$$C_f = \frac{1}{\left(1 + 4 \cdot Fo + h_g \cdot C_t\right)} \tag{13}$$

Solar cells have negligible thickness and their thermal resistance is neglected, therefore only their optical properties are modelled. The on-board printed circuit boards and the batteries are modelled as lumped nodes. This approach has simplified the calculation of the view factors to a great extent but, on the other side, the temperatures calculated so far represent average values and cannot account for local hot spots.

The most critical components are the batteries, because they can work only in a small temperature range (see Table 2). The lumped approach can be accepted for batteries, as heat generation is spread on their volume. The batteries are packed between two thin (0.5 mm) aluminium plates, which are not modelled with regard to thermal conduction because their contribution is negligible, while their optical properties are considered in the radiative model. Thermal radiation inside the satellite is modelled with the Absorption Factor Method. The internal volume of the satellite is subdivided into four cavities; for every cavity a matrix is calculated, which combines the geometrical (i.e. areas) and optical (i.e. absorption factors, emissivity) properties of the enclosure.

For instance, the temperature of the board S1 at time $l + 1$ is obtained with the following heat balance equation:

$$\left(-2\varepsilon_{S1} \cdot A_{S1} + eAB_{S1}(2,1) + eAB_{S1}(1,2)\right) \cdot \sigma \cdot \left(T_{S1}^{(l+1)}\right)^4 - \left(\frac{m_{S1} \cdot c_{S1}}{\Delta\tau} + h_{S1}\right) \cdot T_{S1}^{(l+1)} + \dot{Q}_{int} + \frac{m_{S1} \cdot c_{S1}}{\Delta\tau} \cdot T_{S1}^{(l)} \tag{14}$$
$$+ \sigma \sum_{w=1}^{z} \left(\left(1 - \delta_1(k)\right) \cdot eAB_{S1}(w,1) \cdot T_{cav,S1}^4(1,w) + \left(1 - \delta_2(w)\right) \cdot eAB_{S1}(w,2) \cdot T_{cav,S1}^4(2,w)\right) = 0$$

where $[eAB_{S1}]$ is a matrix wherein elements represent the energy absorbed by S1 in every cavity delimited by S1, and $[T_{cav}]$ is a matrix wherein rows are the temperatures of the surfaces of the cavities delimited by S1. Every internal node has its own $[T_{cav}]$ matrix.

The coefficient 2 in the first term of Eq. (14) indicates that both sides of S1 are involved in the radiative heat transfer. The Kronecker δ vectors specify that S1 corresponds to the second surface in the first cavity (C2, δ_1), hence the notation $eAB_{S1}(2,1)$, while it corresponds to the first surface in the second cavity (C3, δ_2), hence the notation $eAB_{S1}(1,2)$. h_{S1} is the thermal conductance between S1 and the

mounting bar, $T_{\text{sup}}^{(l+1)}$ is the temperature of the corresponding node of the mounting bar, while $\dot{Q}_{\text{int}}$ is the internal heat rate in S1.

The flow chart of the numerical code is shown in Figure 9. The code is composed by nineteen MATLAB® functions and by a C++ script that calculates the quantities related to the terrestrial magnetic field, which are imported in the main MATLAB® script.

The numerical procedure can be basically summarised as follows: for every time step the program determines the position of the satellite on orbit and the orientation of its faces with respect to the Earth and the Sun, which is preliminary to the calculation of the external radiation (IR terrestrial radiation, solar radiation and albedo). These quantities, together with the on-board energy sources and the temperatures at time l, are used to calculate the temperatures at time $l+1$ in an iterative loop until convergence.

5. **Thermal analysis: results and discussion**

Temperature profiles can be calculated and displayed for each node making use of the simulation code. The following graphs refer to a circular orbit, with an inclination equal to 98 deg and an altitude of 600 km, which has been analysed for the worst cold and the worst hot cases. The results refer to the satellite configuration with a full passive thermal control system, realised with multilayer Kapton® insulation, selective coatings and heat sinks. Thermo-physical and optical properties of materials are discussed in detail in Section 5.3. The assumed time step is equal to $\Delta\tau = 10$ s. Each external surface of the satellite is discretized with a uniform hexa grid divided into 64 nodes. The mounting bars of the electronic stack are modelled as 13 nodes, and the connection rods of S0 are modelled as 3 nodes. The electronic boards and battery packages are modelled with a lumped node approach.
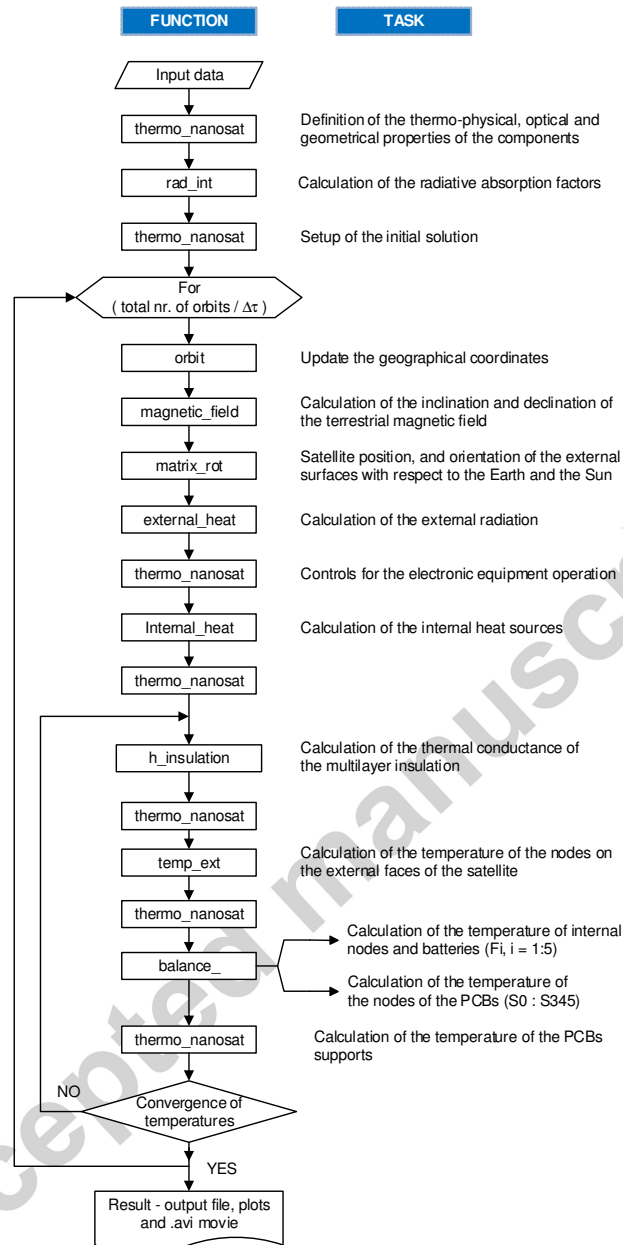
Figure 9: flow chart of the simulation code

5.1. Results

The following graphs show the temperature profiles during four orbits: the first two orbits are influenced by the initial conditions, while the remaining orbits are stabilised.

Figure 10 illustrates the temperature profiles of the central node of each external face of the nanosatellite. The central node has been selected as the most representative of the average condition of the whole surface. The video, generated by the numerical simulation code, is useful to observe the variation of temperature of all external nodes. The graphs show that the temperature range for each revolution is about 50 °C. Figure 11 illustrates two intermediate cases, a hot orbit with electronics switched off (right-hand graph), and a cold orbit with electronics on (left-hand graph). By comparison of

Figure 10 and Figure 11 it can be noticed that in the cold case switching electronics on leads to an increase of the average temperature of about 5 °C. In a similar way, temperature decreases by 5 °C in the hot case with electronics switched off, however this condition represents an off-nominal operative mode of the satellite.
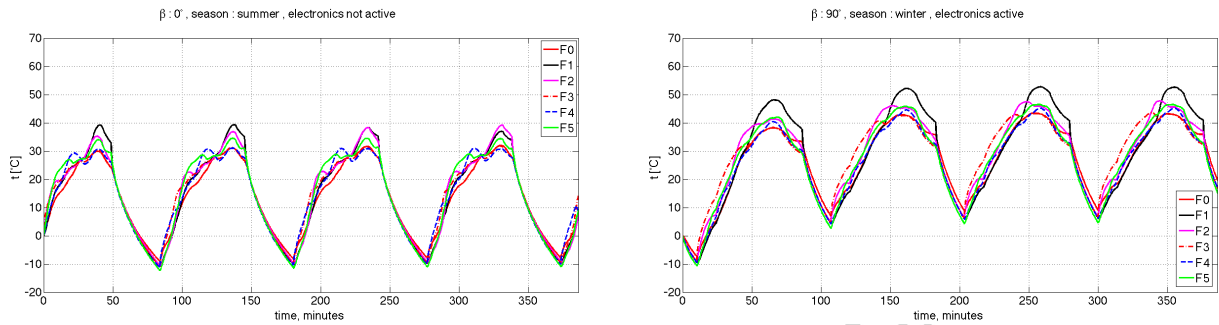

Figure 10: temperature profiles of the central node of each external face for worst cases along four orbits. On the left: worst cold case; on the right: worst hot case.
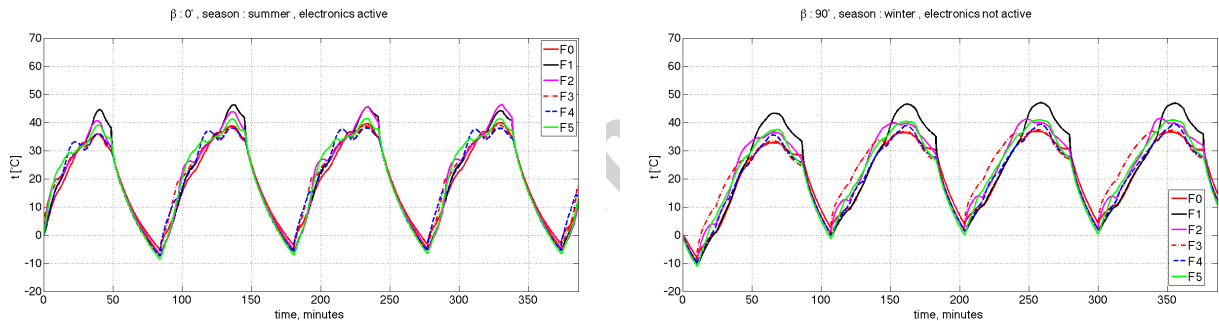

Figure 11: temperature profiles of the central node of each external face for two intermediate conditions along four orbits. On the left: orbits with $\beta = 0$ deg and Earth @aphelion, electronics ON (practical cold case); on the right: orbits with $\beta = 90$ deg and Earth @perihelion, electronics OFF (off-nominal hot case).

Figure 12 shows the temperature profiles of the batteries for the worst hot and cold cases. The temperature range is greater for the orbit with $\beta = 0$ deg ($\Delta T \sim 30$ °C) compared to $\beta = 90$ deg ($\Delta T \sim 20$ °C); for the hot case, the temperature range limits for the batteries are satisfied (cf. Table 2), albeit with a small margin for LiPo batteries, under any operating conditions (charge, discharge, stand-by). In the cold case instead, the temperature limits are not met in the recharge phase. The minimum temperature of the worst cold case is achieved when the satellite is in eclipse, and the battery is not charging. However, at the end of the eclipse the battery may start charging outside its operating temperature range, and this could lead to damage it. A simulation of the cold case with electronics active was performed, and the results show that the batteries are within the range of temperatures at any operating condition. This intermediate case is more realistic with respect to the worst cold case. In fact in the latter case electronics is considered as completely switched off (no thermal loads), even though this is not a nominal mode of operation and it may occur only in case of a serious failure, which would anyway compromise the mission, notwithstanding thermal issues. Figure 13 shows the temperature

profiles of the electronic boards and the brushless DC motor, which result within the required temperature limits with an adequate margin. The RxTx and the Power Switch electronic boards experience the highest temperature peaks. Heat sinks are therefore suggested for both these boards. The low temperatures that are reached in the worst cold case are not critical.
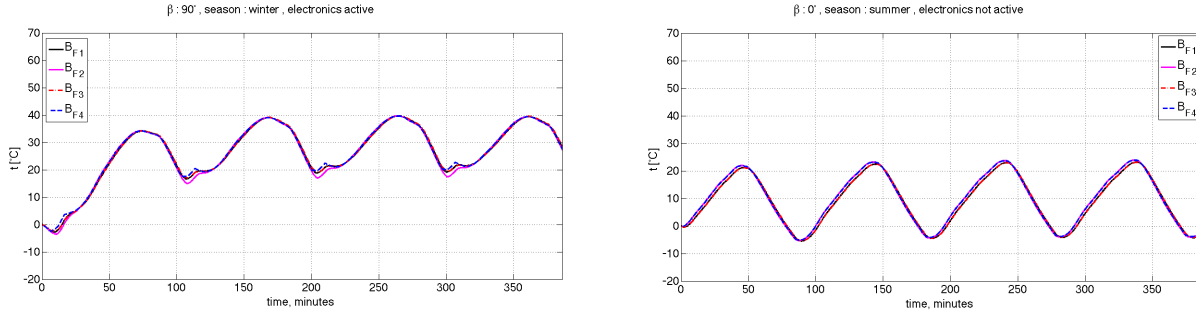

Figure 12: temperature profile of batteries. On the left: worst hot case; on the right: worst cold case
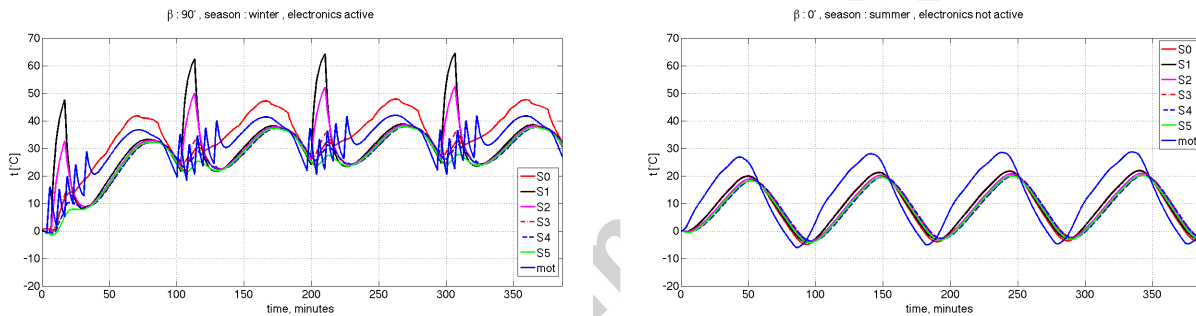

Figure 13: temperature profile of electronic boards and brushless motor along four orbits. On the left: worst hot case; on the right: worst cold case

Figure 14 illustrates the temperatures of the nodes of the bars that support the electronic stacks. In the graph relative to the hot case (left) the peaks related to the operation of RxTx and Power Switch are clear.
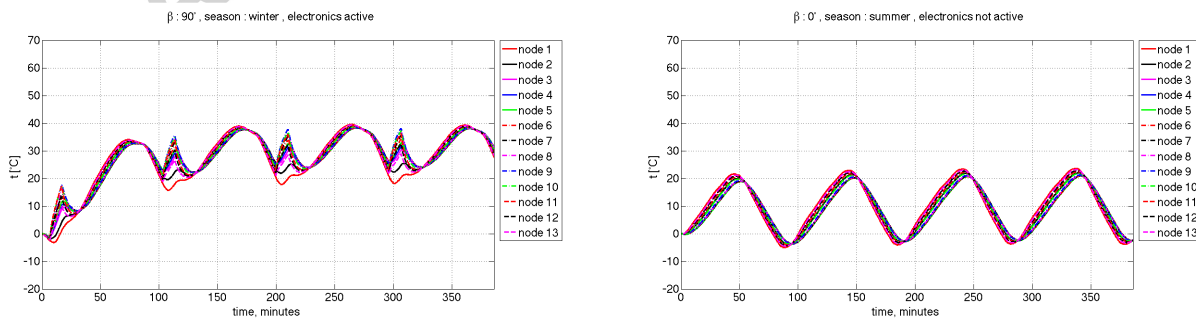

Figure 14: temperature profile of boards mounting bars. On the left: worst hot case; on the right: worst cold case (4 orbits, height 600 km, i = 98 deg)

5.2. Validation of the code

The results of the thermal analysis were compared to ESATAN-TMS® analyses to investigate the correlation between the two models. The comparison between ESATAN-TMS® and MATLAB® results was based on a circular orbit with 98 deg inclination, 600 km altitude.

In ESATAN-TMS® the approach for computing the external radiative exchange factors is numerical and based on Monte-Carlo ray-tracing, with a default configuration of 10,000 rays firing from each surface. The MATLAB® routine calculates internal exchange factors after the definition of thermo-physical, optical and geometrical properties of the components, while external fluxes are calculated in the "for" loop, as discussed in Section 4.1 and shown in the flow chart in Figure 10. ESATAN-TMS® radiative module ensures a moderate computation time in the range of 180s for one orbit when considering a model with a good level of detail (approximately 150 nodes). However no significant changes in external fluxes have been recorded among the different nodes of the same surface in the case of the nanosatellite geometry scale. For instance, the average incident solar fluxes calculated with ESATAN-TMS® for 25 nodes on the external faces F1 and F3 differ from the value calculated with the MATLAB® routine for one single lumped parameter node by a maximum error of 2%. A higher error has been recorded for the incident albedo and Earth IR radiation, for which ESATAN-TMS® results deviate from MATLAB® ones by a maximum of 9%. This error can be traced back to the view factors calculation and would require further investigation; nevertheless this is considered a second order effect with respect to the values of solar direct fluxes impinging the surface.

The temperatures of the satellite obtained with the developed code were compared to an ESATAN-TMS® analysis, using a less detailed but yet comparable geometrical model shown in Figure 15. The temperature distribution of a battery in the worst cold case is reported in Figure 16 as an example. The temperatures show the same trend, with a ±3 °C maximum error. The results differ by a negligible shift in the eclipse start time, due to a different orbit modelling and transient computation between the two tools. ESATAN-TMS® model requires the setup of a transient solution with a time-step of 0.01 s to converge. The time-step is limited by the minimum value of the ratio of nodal capacitance to sum of conductance (CSGMIN parameter), which draws to a high computational cost, with the advantage of a better spatial resolution in the calculus. This resolution however results to be unnecessary for the geometrical scale under examination, and does not lead to significantly different results compared to the more agile MATLAB® analysis. The total running time for six orbits is of the order of 3000 s and 700 s for ESATAN-TMS® and MATLAB® respectively
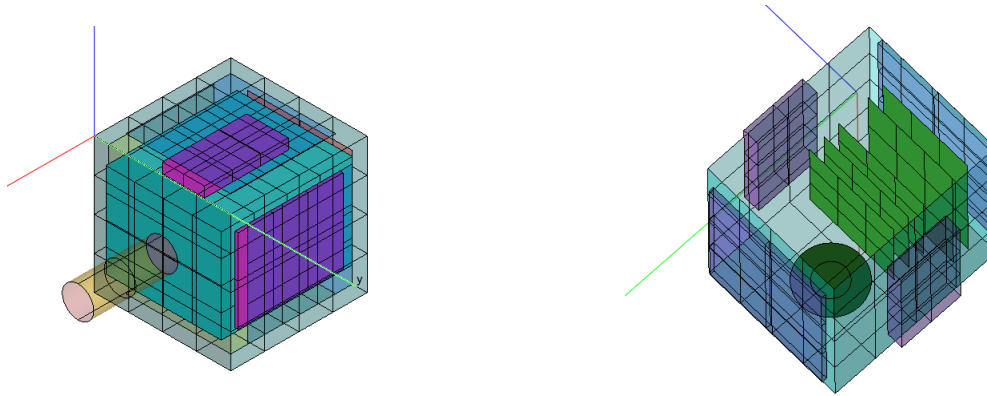
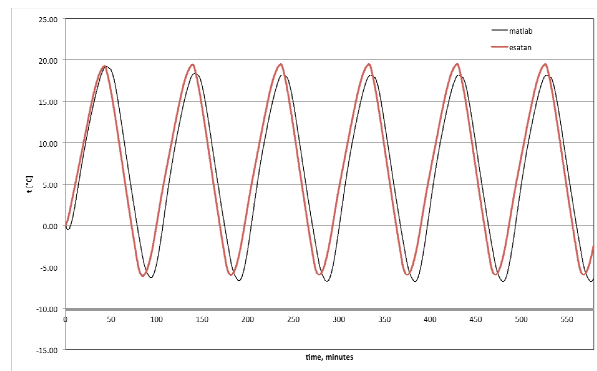Figure 15: satellite ESATAN-TMS® geometrical model

Figure 16: comparison of battery temperature profile with MATLAB® and ESATAN-TMS®

5.3. Discussion on thermal control strategy

The process of thermal analysis has provided the design of the nanosatellite with useful indications. Given the nanosatellite configuration and the components characteristics, the hot case represents the most critical condition. In particular, the batteries exceed their upper temperature limit if not adequately protected. Hereafter the strategies adopted in order to meet the thermal requirements are described and discussed.

The analysis moved from an initial satellite configuration with a passive thermal control system, given a fixed satellite architecture and an invariable internal components' layout. Conductive and radiative properties of materials have been adjusted and traded-off over several simulation runs, by means of an optimization process aimed at meeting a design point, to which the results presented in Section 5.1 pertain.

As far as the external structure is concerned, being the aluminium an excellent conductor, it contributes to level out the temperature of the panels. However, heat transfer is limited by the optical properties (solar absorptivity $\alpha = 0.1$ and infrared emissivity $\varepsilon = 0.06$). To improve the external heat transfer, we modified the optical properties of the external surfaces not occupied by solar cells, antennas and cameras' lenses, increasing infrared emissivity while keeping the solar absorptivity relatively low. As a result of the thermal analysis, the desired optical properties vary in the range of $\alpha = 0.2 \div 0.3$ and $\varepsilon =$

0.8÷0.9.To meet this design point, the feasible solutions identified are surface treatments (e.g. oxidation), surface coatings (e.g. paints) or surface overlay by means of specific tapes. Surface treatments are usually complex and expensive, oxidation is not electrically conductive, and it could lead to a major design limitation if not specifically required. Coatings, usually black or white, can be either electrically conductive or not. For our purpose, white coatings (α = 0.2÷0.5, ε = 0.8) are preferable to the black ones (α = 0.9, ε = 0.88). Similar performances can be achieved with the use of specific tapes with a Teflon® substrate covered by a deposit of aluminium (α = 0.3, ε = 0.8). Since paints are more critical in terms of outgassing, the use of a specific tape overlay is recommended.

As far as the internal configuration is concerned, insulation can be properly achieved by reducing thermal conductivity and IR emissivity at the interfaces. Different Multi-Layer Insulation (MLI) materials have been traded along the thermal analysis (k = 0.02÷0.1 W/mK, ε = 0.01÷0.03). Ten layers-MLI blankets are recommended between external and internal aluminium panels. The internal support structure is made of aluminium and it reflects great part of the heat dissipated by the electronics, which therefore tend to warm up. In order to avoid excessive temperatures, two main actions can be undertaken: to increase the IR emissivity of the aluminium panels that face the interior of the satellite, and to increase the thermal conductivity of the electronic boards.

As resulted from the simulation process, a value of emissivity equal to ε = 0.8 has been selected for the panels of the internal structure. The feasible solutions may include a chromic/sulphuric anodizing surface treatment or, alternatively, the use of special black paints, i.e.:

- Aeroglaze Z306, which has negligible electrical conductivity and appropriate outgassing level
- Aeroglaze Z307, which has not negligible electrical conductivity and little higher outgassing level, if compared to the previous

In order to improve heat dissipation of the electronic boards, a heat sink may be applied (in particular on the RxTx and the Power Switch boards), to increase the thermal conductivity of FR-4 (k = 0.25 W/mK) to a value in the range 1.0÷4.0 W/mK. Taking into account the small size of the boards and the type of connections between their components, traditional metallic heat sinks (1-mm thick aluminium or copper sheets) cannot be used. A good alternative is represented by printed heat sinks, whose characteristics are described in detail in [29]. They consist of a paste based on a special polymeric matrix filled with finely scattered particles which guarantee the required heat-conductive properties. Furthermore, the process of application is less complex and can be more easily automated, if compared to traditional metallic heat sinks.

The results showed that a basically passive control is sufficient to maintain most spacecraft's components within their temperature range with appropriate insulation, thermal coatings or tapes overlay solutions. Batteries still remain critical also in the coldest conditions. However, it is worth reminding that the worst cold case is not a nominal mode of operation because electronics is considered completely switched off, which means a serious failure of the mission. A major problem may rather arise in case of a sudden transition from eclipse to sunlight, and therefore from the discharge phase to the charge phase, which requires a minimum operative temperature of 0 °C. For these reasons, the use of heaters to warm up batteries is recommended. Heaters operating according to an on/off switch cycle are sufficient in order to meet the requirements while keeping the TCS as simple as possible.

6. Conclusions

The results of the thermal analysis have turned out to be extremely useful in the framework of the PiCPoT project. Taking into account the obtained results, the satellite has been partially modified, in order to meet all temperature requirements. The satellite has then been successfully tested in a thermo-vacuum chamber.

The numerical simulation code has been designed and implemented specifically for the project but, thanks to its flexibility, it is well suited for other similar projects. The code allows to customise input parameters such as:

- physical, thermal and optical properties of materials
- geometry of the satellite
- external heat sources (solar radiation, albedo and Earth IR radiation)
- internal heat loads (power dissipated and duty cycles)
- orbit parameters (altitude and inclination)
- lighting conditions (Earth's position along the ecliptic and β angle)
- number of orbits
- number of nodes for the external surfaces
- time step

The comparison with professional thermal analysis software (ESATAN-TMS®) verified the goodness of the approach implemented and validated the tool for future applications. The code does not aim at competing with commercial solutions, rather it is intended to complement the existing offer with an efficient nanosatellite-scale tool for thermal analysis.

The numerical simulation code is integrated into a wide mission simulation program, which encompasses the simulation of the mission and the system from different points of view. In particular some modules that are strictly related to the presented thermal analysis are worth mentioning: the simulation of the orbit and the satellite's attitude, the parametric modelling of the geometry of the satellite, and the functional simulation of the operative modes. The integration of the different simulation modules is one of the research activities that are currently in progress, in order to optimize procedures and build up a flexible, multi-purpose and global mission analysis tool.

A. Symbols
Latin letters

a   thermal diffusivity, m^2/s

A   area, m^2

B   radiative absorption factor

c   heat capacity at constant pressure, J/kgK

d   distance between two nodes of the grid, m

e   orbit eccentricity

F   view factor

Fo   Fourier number

h   thermal conductance, W/m^2K

IR   infrared Earth radiation ($239\ W/m^2$)

i   orbital inclination angle

k   thermal conductivity, W/mK

m   mass, kg

$\dot{q}_v$ volumetric heat flux, W/m^3

$\dot{q}_s$ heat flux, W/m^2

$\dot{Q}$ heat rate, W

r   radiative reflectivity

R   distance between the satellite and the Earth's centre

RE   Earth radius

s   material thickness, m

S   Solar radiation, W/m^2

T   temperature, K
x, y, z   spatial coordinates

Greek letters

α   albedo (0.29)

β   orbital angle between the orbit and the Sun-Earth vector

γ   angle between the Earth-satellite vector and the perpendicular to the satellite external face

δ   Kronecker delta

Δτ   time step, s

ε   emissivity

θ   solar zenith angle, the angle between the Earth-satellite and the Earth-Sun directions

ι   angle between the Earth-satellite vector and the tangent to the Earth viewed from the satellite

ρ   density, kg/m^3

σ   Stefan-Boltzmann constant (5.67x10^{-8} W m^{-2} K^{-4})

ζ   angle between a surface and the vector opposite to solar radiation

τ   time, s

Subscripts

α   albedo

cav   cavity

i, j   *i*-th, *j*-th element

int   inside the satellite

IR   Infrared Earth radiation

g   gap between two nodes

sun   solar

S1   electronic board nr.1

References

[1] R. Sandau, Status and trends of small satellite missions for Earth observation, Acta Astronautica, 66 (1-2) (2010) 1–12

[2] D. Selva, D. Krejci, A survey and assessment of the capabilities of Cubesats for Earth observation, Acta Astronautica 74 (5-6) (2012) 50–68

[3] J. Bouwmeester, J. Guo, Survey of worldwide pico- and nanosatellite missions, distributions and subsystem technology, Acta Astronautica 67 (7-8) (2010) 854–862

[4] H. Heidt, J. Puig-Suari, A.S. Moore, S. Nakasuka, R.J. Twiggs, CubeSat: A New Generation of Picosatellite for Education and Industry Low-Cost Space Experimentation, in: Proceedings of 14th Annual USU Conference on Small Satellites, Logan, UT, 2000

[5] CubeSat Design Specification, Revision 13, Updated 2-20-2014 [online] http://www.cubesat.org/index.php/documents/developers. Last access: November 2014

[6] S. Corpino, S. Chiesa, N. Viola, PiCPoT program: lessons learned, In: Proceeding of 58th International Astronautical Congress, Hyderabad, India, Sept. 24-28, 2007

[7] Interface Control Document for BelKA SC, Baumanets SC, UniSat-4 SC, PiCPoT SC, P-Pod containers with CubeSat SC and Dnepr Launch Vehicle, Doc. No. DNR YZH ICD 001 00, issue 1, (2005)

[8] D.G. Gilmore, Spacecraft thermal control handbook, vol. 1. 2nd ed., The Aerospace Corporation, AIAA, 2002

[9] R. Lyle, P. Stabekis, R. Stroud, Spacecraft Thermal Control – NASA Space Vehicle Design Criteria (environment), NASA SP-8105

[10] C.J. Fong, Lessons learned of NSPO's picosatellite mission: YamSat – 1A, 1B, and 1C, in: Proceedings of the 16th Annual/USU Conference on Small Satellite, Logan, UT, 2002

[11] J.A. Schaffner, The electrical system design, analysis, integration and construction of the CalPoly State University CP1 CubeSat, in: Proceedings of the 16th Annual/USU Conference on Small Satellite, Logan, UT, 2002

[12] T. Brauneis, Ionic sCintillation Experiment, CUBEsat Project, in: Proceedings of 1st Annual CubeSat Workshop, San Luis Obispo, CA, 2004

[13] S. Czernik, Design of the thermal control system for Compass-1, Diploma Thesis. Aachen University of Applied Science, 2004

[14] M.F. Diaz-Aguado, J. Greenbaum, W.T. Fowler, E.G. Lightsey, Small satellite thermal design, test, and analysis, in: Proceedings of SPIE 6221, Modeling, Simulation, and Verification of Space-based Systems III, Orlando (Kissimmee), FL, 2006

[15] L. Jacques, Thermal Design of the OUFTI-I nanosatellite, Master Thesis. University of Liege, 2009

[16] J. Yoo, H. Jin, J. Seon, Y. Jeong, D. Glaser, D. Lee, et al., Thermal analysis of TRIO-CINEMA mission, Journal of Astronomy and Space Sciences. 29 (2012) 23–31

[17] D.R. Wilkes, Thermal Control Surfaces Experiment, NASA CR 1999-209008 (1999)

[18] R.R. Kamenetzky, J.A. Vaughn, M.M. Finckenor, R.C. Linton, Evaluation of Thermal Control Coatings and Polymeric Materials Exposed to Ground Simulated Atomic Oxygen and Vacuum Ultraviolet Radiation, NASA TP-3595 (1995)

[19] M. Finckenor, D. Dooling, Multilayer insulation Material Guidelines, NASA TP-1999-209263 (1999)

[20] M.P. Thekaehara, Solar Electromagnetic Radiation – NASA Space Vehicle Design Criteria (environment), NASA SP-8005 REV (1971)

[21] B. Anderson, C. Justus, G. Batts, Guidelines for the selection of near-earth thermal environment parameters for spacecraft design, NASA TM-2001-211221 (2001)

[22] C.G. Justus, G.W. Batts, B.J. Anderson, B.F. James, Simple Thermal User's Guide Environment Model (STEM), NASA TM-2001-211222 (2001)

[23] R. Lyle, J. Leach, L. Shubin, Earth Albedo and Emitted Radiation – NASA Space Vehicle Design Criteria (environment), NASA SP-8067 (1971)

[24] B. Gebhart, Heat Transfer, McGraw-Hill, 1971

[25] R. Siegel, J.R. Howell, Thermal Radiation Heat Transfer, 3rd ed., Hemisphere, 1992

[26] M.N. Ozisik, Radiative Transfer and interaction with conduction and convection, John Wiley & Sons, 1973

[27] Y. Jaluria, K. Torance, Computational Heat Tranfer, 2nd ed., Taylor and Francis, 2003

[28] M.N. Ozisik, Heat Conduction, John Wiley & Sons, 1980

[29] M. Suppa, The use of printed heat sinks to solve thermal problems on printed circuit boards, in: Proceedings of the 8th FED Conference, Beirut, Lebanon, 2000

Vitae

Sabrina Corpino has been working as Assistant Professor at the Department of Mechanical and Aerospace Engineering (DIMEAS) at Politecnico di Torino since July 2003. Since 2011 she is Professore Aggregato with tenure of "Space systems and missions design" of the Master degree in Aerospace Engineering.

She is responsible for all satellites' programs developed by the Aerospace Systems Engineering Team, ASSET. She is program manager of the CubeSat program at Politecnico di Torino, which involves other researchers and many students.

Her main scientific interests are: Systems of Systems analysis, Design Methodologies for Aerospace Systems, Techniques for systems simulation and verification.

Matteo Caldera, mechanical engineer and Ph.D. in Energy, is currently researcher in the Italian energy agency ENEA. He worked as post-doc research fellow in the Energy Department (DENERG) of Politecnico di Torino. His MS thesis was focused on the development of the numerical models for the thermal analysis of the PiCPoT nanosatellite, and earned the national first prize in thermal-fluid-dynamics. His research activities include CFD and thermal simulations, design optimisation, development of methodologies for the analysis of renewable energy systems.

Marco Masoero (Torino, 1954) holds degrees in Civil Egineering from Politecnico di Torino, Italy (Laurea, 1977) and in Mechanical and Aerospace Engineering from Princeton University, USA (MSE, 1982). Since 1983 he has been part of the engineering faculty of Politecnico di Torino, where he is presently Professor of Technical Physics and Head of the Department of Energy. His research, teaching and consulting activities are focused on energy efficiency in buildings, HVAC design, numerical analysis of thermal systems and engineering acoustics.

Fabio Nichele is a Ph.D. student at Politecnico di Torino. His research activities include system-of-systems analysis, study of evolving space programs, integration of new systems within existing architectures. He has been working with ASSET and CubeSat Team of the Mechanical and Aerospace Department of Politecnico di Torino since 2009, working on small satellite projects. He had been involved in the design, verification and launch campaign of e-st@r satellite. Fabio Nichele is author of papers published in conference proceedings, and he is currently involved as teaching assistant for the course "Space missions and systems design" of the Aerospace Engineering degree.

Nicole Viola has been working as Assistant Professor at the Department of Mechanical and Aerospace Engineering at Politecnico di Torino since March 2008. She had been working as Researcher on aeronautics and space systems design at Politecnico di Torino from April 2000. She got her Ph.D. in Aerospace Engineering in 2004 on "Conceptual definition of trans-atmospheric and space vehicles". She is author of papers published on books, journals and international and national proceedings. Nicole Viola is currently teacher with tenure of the undergraduate course "On-board equipment and avionic systems" of the Aerospace Engineering degree.